JOURNAL OF Materials Feature Article CHEMISTRY

Layered molecular optoelectronic assemblies

Itamar Willner* and Bilha Willner

Institute of Chemistry and The Farkas Center for Light-Induced Processes, The Hebrew University of Jerusalem, Jerusalem 91904, Israel. E-mail: willnea@vms.huji.ac.il

Received 2nd June 1998; Accepted 20th August 1998

Layered functionalized electrodes are used as optoelectronic assemblies for the electronic transduction of recorded photonic signals. Functionalization of a Au electrode with a photoisomerizable redox-activated monolayer enables the amperometric transduction of the photonic information recorded by the interface. This is exemplified with the organization of a phenoxynaphthacenequinone monolayer (1a). Organization of a photoactivated command layer on an electrode can be used to control interfacial electron transfer and might be applied for the electrical transduction of recorded optical signals. This is addressed with the assembly of a nitrospiropyran photoisomerizable monolayer (2a) on a Au electrode which acts as a command surface for controlling by light interfacial electron transfer. The monolayer undergoes photoisomerization between the neutral state (2a) and the positively charged protonated merocyanine state (2b). The charged interface controls the oxidation of dihydroxyphenylacetic acid, DHPAA (3), and of 3-hydroxytyramine, DOPA (4), and the system is used for the electrochemical transduction of optical signals recorded by the monolayer. Functionalization of electrodes with a β-cyclodextrin monolayer or with an eosin π-donor layer enables the light-stimulated association or dissociation of the photoisomerizable *N,N′*-bipyridinium azobenzene (5*t*) and of bis-pyridinium azobenzene (8t) to or from the modified surfaces. Association and dissociation of the surface-associated supramolecular complexes are transduced by electrochemical or piezoelectrical signal outputs. The organization of a supramolecular system where a molecular component is translocated by light-signals between two distinct positions enables one to design 'molecular machines'. This is exemplified by the organization of a molecular assembly consisting of a ferrocene-functionalized β-cyclodextrin (11) threaded onto an azobenzene-alkyl chain wire and stoppered with an anthracene barrier which acts as a nanoscale molecular machine, a light-stimulated 'molecular train'. The ferrocene-functionalized β-cyclodextrin is reversibly translocated between the *trans*-azobenzene and the alkyl chain by cyclic light-induced isomerization of the photoactive monolayer. The position of the β-cyclodextrin receptor is transduced by its chronoamperometric response.

Miniaturization of devices to the molecular level or nanoscale dimensions represents one of the most challenging research subjects in modern science.[1,2] Progress in tailoring molecular machines may have important implications in molecular-based logic gates,[3] computer technologies,[4,5] sensory methods,[6] bioengineering[7] and biomimetic architecture.[8] The organization of molecular devices requires the assembly of integrated molecular systems exhibiting several elements: (i) The molecular assembly should communicate with its macroscopic environment. That is, external signals should activate the physicochemical functions of the molecular system. External signals that activate the molecular systems may include photonic signals, electrical signals, magnetic inputs *etc.* (ii) The molecular assembly should respond to the external triggering signals by altering its physicochemical properties. Activation of binding processes,[9,10] translocation,[11] redox properties,[12] catalytic reactions[13] *etc.* represent chemical functions that are triggered by external signals. (iii) The functions of the molecular device should be externally controlled. That is, external signals block the chemical functions of the system and regenerate the device for a secondary operation cycle. (iv) The molecular device should include a transduction element that provides information-transfer from the molecular system to the macroscopic environment regarding its physicochemical state, *e.g.* sensory level, chemical state or structural position. The transduction signals may include, for example, optical, electrical, or piezoelectrical signals.

Molecular switches,[14,15] molecular brakes,[16] molecular ratchets[17] and molecular shuttles[18] represent a few chemical assemblies duplicating the functions of macroscopic devices. Electrochemical,[12,19] photonic,[14,20] thermal[21] and pH[22] signals were used to trigger molecular devices. For example, a bis-bipyridinium cyclophane threaded and stoppered on a *p*-phenylenediamine-*p*-dialkoxybiphenyl wire is reversibly translocated on the molecular wire by cyclic oxidation and reduction of the π-donor diamine unit, Fig. 1(A).[18*a*] Light-stimulated association and dissociation of ions,[9,23] *e.g.* Fig. 1(B),[23*b*] to photoisomerizable receptors represents a light-activated ion switch. Oxidation or reduction of a metal ion may induce its internal translocation between two ligation sites,[15*b*] respectively [Fig. 1(C)]. However, most of the reported systems are not integrated in a configuration meeting all the characteristic elements of molecular devices. The systems were assembled as supramolecular complexes in solution, and their signal-triggered properties were monitored by different spectroscopic means.

Among the possible molecular devices, photoactivated molecular switches or phototriggered molecular machines play a central role in future nanoscale optoelectronics. Tailoring of photoactivated molecular switches (PMSs) requires the integration of a light-sensitive chemical assembly with a solid support acting as a transduction element. Photochemically-induced excitation, electron transfer,[24] or isomerization of the chemical component,[25] stimulate electronic redox or structural changes in the chemical component. These chemical perturbations are electronically transduced by the solid support, *e.g.* by amperometric, potentiometric, conductometric, impedance or piezoelectric signals. Photoactive or electroactive chemical functionalities were assembled on solid supports by polymerization or layer deposition of thin films.[26] Covalent association of monolayers onto surfaces,[27] and specifically, the linkage of thiolated monolayers to metal supports, *e.g.* Au surfaces,[28,29] opens the possibility of organizing ordered two-dimensional monolayer arrays on solid surfaces. We have recently discussed our activities in tailoring optobioelectronic devices by the assembly of bioactive monolayers[30,31] on electrode supports. The functions of the integrated biomaterial/transducer systems in the electronic transduction and amplification of recorded optical signals[32,33] as well as biosensor[34] and bioelectronic[35] applications were addressed.

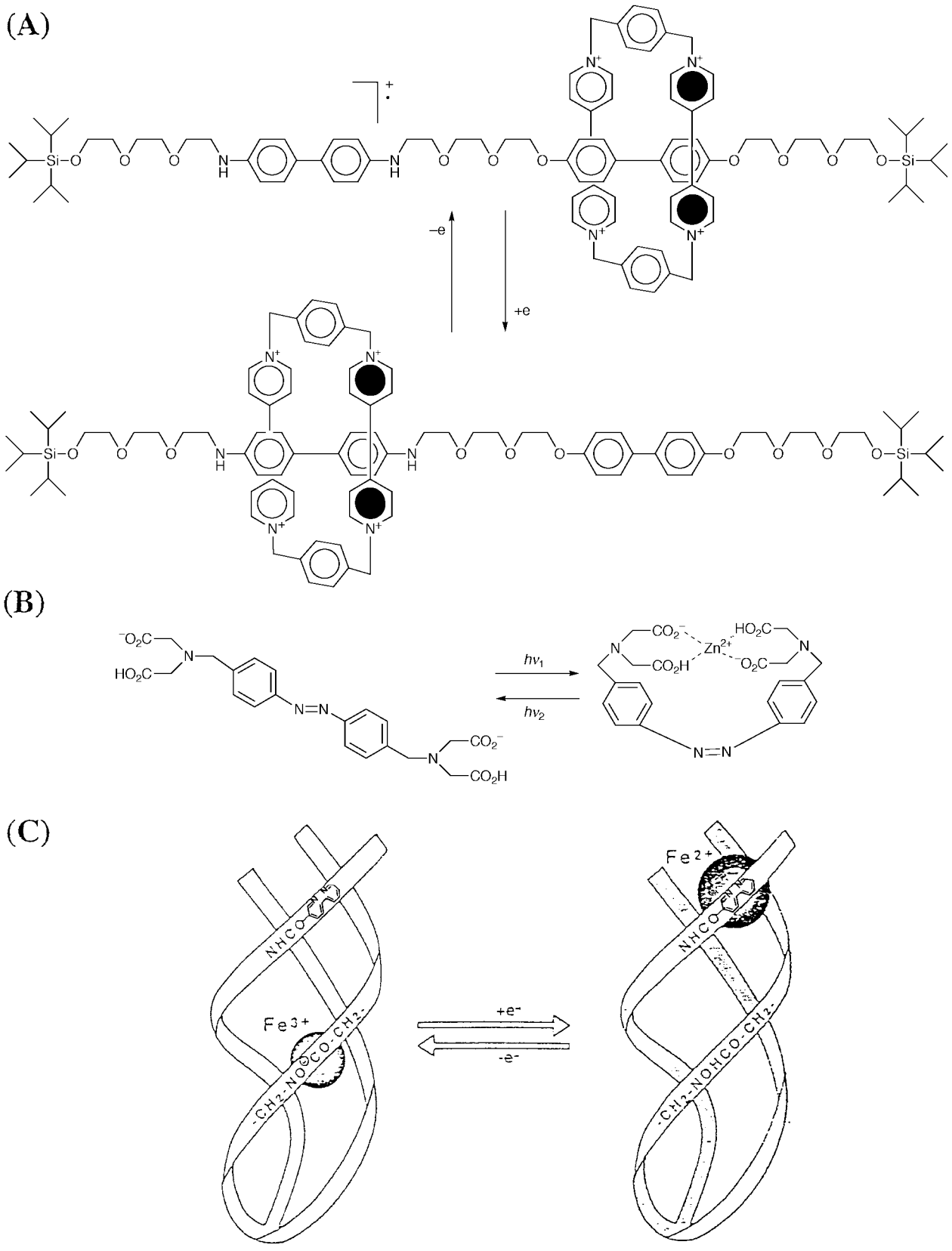

Fig. 1 Signal-controlled chemical switches: (A) Reversible electrochemical translocation of an electron acceptor between two distinct electron donor sites. (B) Reversible photochemical binding and dissociation of ions by a photoisomerizable ion-chelator. (C) Electrochemical translocation of an ion between distinct ligation sites.

The present article summarizes recent progress in the organization of molecular optoelectronic systems and, specifically, PMS devices and phototriggered molecular machines, using photoisomerizable chemical components as the active ingredient for recording the photonic information. We emphasize the integration of molecular optoelectronic systems by the assembly of thiolated monolayers on Au surfaces for the electrochemical or piezoelectric transduction of the photonic signals.

Tailoring of integrated molecular optoelectronic assemblies that act as PMSs was achieved by three general approaches schematically outlined in Fig. 2. One approach involves the

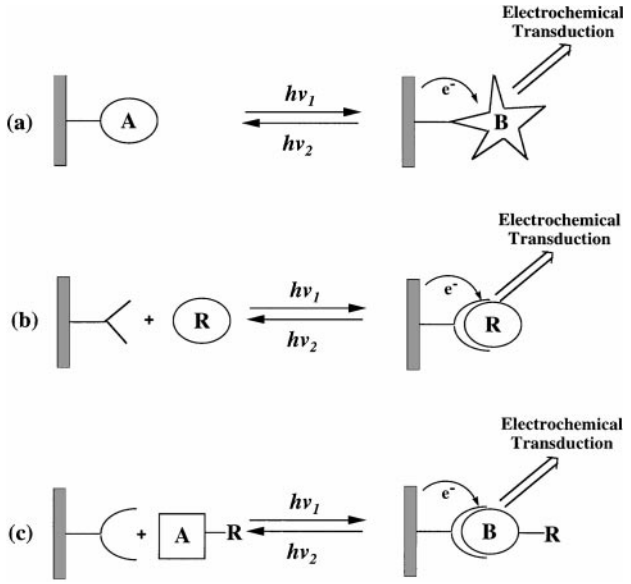

Fig. 2 Schematic configuration of photoactivated molecular switches: (a) Redox activation of a photoisomerizable monolayer electrode. (b) Amperometric transduction of light-induced association of a redox-active substrate to a photoisomerizable command interface. (c) Light-induced association of a redox-activated photoisomerizable substrate to a functionalized monolayer electrode.

immobilization of a photoisomerizable component on an electrode as the solid support [Fig. 2(a)]. In the photoisomer state 'A', the molecular unit is redox-inactive and no electronic signal is transduced. Photoisomerization of the chemical component to state 'B' generates a redox-active assembly, and the electron transfer between the electrode and the chemical interface yields the amperometric (electrochemical) transduction of the photonic signal that activates the system. The second approach to organize an integrated photoactivated optoelectronic switch is schematically detailed in Fig. 2(b), and includes the organization of a photoisomerizable monolayer on the solid support that acts as a 'command interface' for controlling electron transfer at the solid interface. In one photoisomer state, electron transfer to a redox probe solubilized in the electrolyte solution is prohibited, whereas in the complementary state of the monolayer the interfacial electron transfer is allowed. The latter process transduces the recorded optical signal as a current output. The third approach to assemble a molecular optoelectronic switch is shown in Fig. 2(c) and involves the assembly of a chemically functionalized surface and its integration with a photoisomerizable molecular component. In configuration 'A' of the molecular component, no affinity interactions with the modified surface exist, and the system is in a mute state. Photoisomerization of the substrate to state 'B' activates the affinity binding of the molecular component to the surface, a process that is electronically transduced (*e.g.* an amperometric, impedance or piezoelectric signal). Our research group has recently exemplified[36] the organization of photoactivated molecular switches (PMSs) based on these concepts, and these 'simple' systems served as a guideline for tailoring more complex nano-structured molecular optoelectronic systems acting as light-driven molecular machines.

Photoisomerizable redox-activated monolayer electrodes

A phenoxynaphthacenequinone monolayer was assembled on a Au electrode as outlined in Scheme 1.[37] A cystamine monolayer was assembled on the Au surface as base monolayer, and 6-[(4-carboxymethylphenyl)oxy]-5,12-naphthacenequinone was covalently linked to the base layer in the presence of 1-ethyl-3-(3-dimethylaminopropyl)carbodiimide (EDC). Fig. 3 (curve a) shows the cyclic voltammogram of the resulting monolayer. An ill-defined redox wave of the *trans*-quinone state (**1a**) is observed. This ill-defined wave is attributed to the fact that a non-densely-packed monolayer of the quinone is formed. Different orientations of the quinone relative to the electrode, or eventually non-specific adsorption of the quinone to the surface, yield a mixture of non-electroactive quinone units and species of different electrochemical features that lead to the broad voltammogram.[38] Treatment of the *trans*-quinone-functionalized electrode with tetradecanethiol ($C_{14}SH$) results in the association of the long-chain, hydrophobic thiolate to surface pinhole defects and the formation of a densely-packed, two-dimensional mixed monolayer consisting of $C_{14}SH$ and the *trans*-quinone.[39] Fig. 3 (curves b–e) show the stepwise rigidification of the quinone component upon treatment of the quinone monolayer with $C_{14}SH$. The quasi-reversible redox wave, $E^{\circ} = -0.62$ V *vs.* SCE (at pH 7.0), is attributed to the two-electron redox process of the *trans*-quinone in a rigidified, aligned configuration in the monolayer assembly. Coulometric assay of the charge associated with the reduction (or oxidation) of the *trans*-quinone component reveals a surface coverage of the electrode by the quinone corresponding to 2×10^{-10} mol cm^{-2}. The electron transfer rate from the electrode to the quinone was estimated to be $k_{et} \approx 2.5$ s^{-1} by following the peak-to-peak separation of the redox wave at different scan rates.

Fig. 4 shows the cyclic voltammogram of the *trans*-quinone monolayer, curve a, and that of the 'ana'-quinone (**1b**) state, curve b, formed upon photoisomerization of the initial monolayer, $305 < \lambda < 320$ nm. In the presence of the 'ana'-quinone monolayer, only the background current of the electrolyte is observed, implying that this photoisomer monolayer is redox-inactive. Irradiation of the 'ana'-quinone monolayer, $\lambda < 430$ nm, restores the *trans*-quinone monolayer and reactivates the amperometric response of the monolayer. By cyclic photoisomerization of the monolayer between the *trans*-quinone and 'ana'-quinone states, the transduced current is switched reversibly between 'ON' and 'OFF' states [Fig. 4 (inset)]. Activation of the electrical redox response of the functionalized monolayer by photonic isomerization of the 'ana'-quinone state to the *trans*-quinone configuration represents the electronic transduction of the recorded optical signal. The back photoisomerization of the *trans*-quinone to the 'ana'-quinone state represents the erasure of the optical signal recorded by the monolayer and the regeneration of the photosensitive recording interface. Thus, the phenoxynaphthacenequinone monolayer assembled onto the Au support exhibits Write-Read-Erase features.

An important aspect in the development of molecular optoelectronic systems involves the amplified electronic transduction of the recorded photonic signals. Such systems could find interesting future applications in designing electronic amplifiers for weak light signals or sensitive actinometers. The photoswitchable redox functions of a photoisomerizable monolayer can be amplified by coupling of the electroactive component to an electron transfer cascade (Scheme 2). The mixed monolayer, consisting of $C_{14}SH$ and the 'ana'-quinone state, provides an insulating layer on the conductive support. This yields a barrier for the direct electron transfer from the electrode to a secondary electron relay solubilized in the electrolyte. Photoisomerization of the monolayer to the *trans*-quinone state activates the vectorial electron transfer from the redox-active unit to the diffusional relay. This stimulates the electrocatalyzed reduction of the relay solubilized in the electrolyte solution. The regeneration of the electroactive quinone unit in the monolayer yields an electrocatalytic cathodic current that represents the amplified amperometric

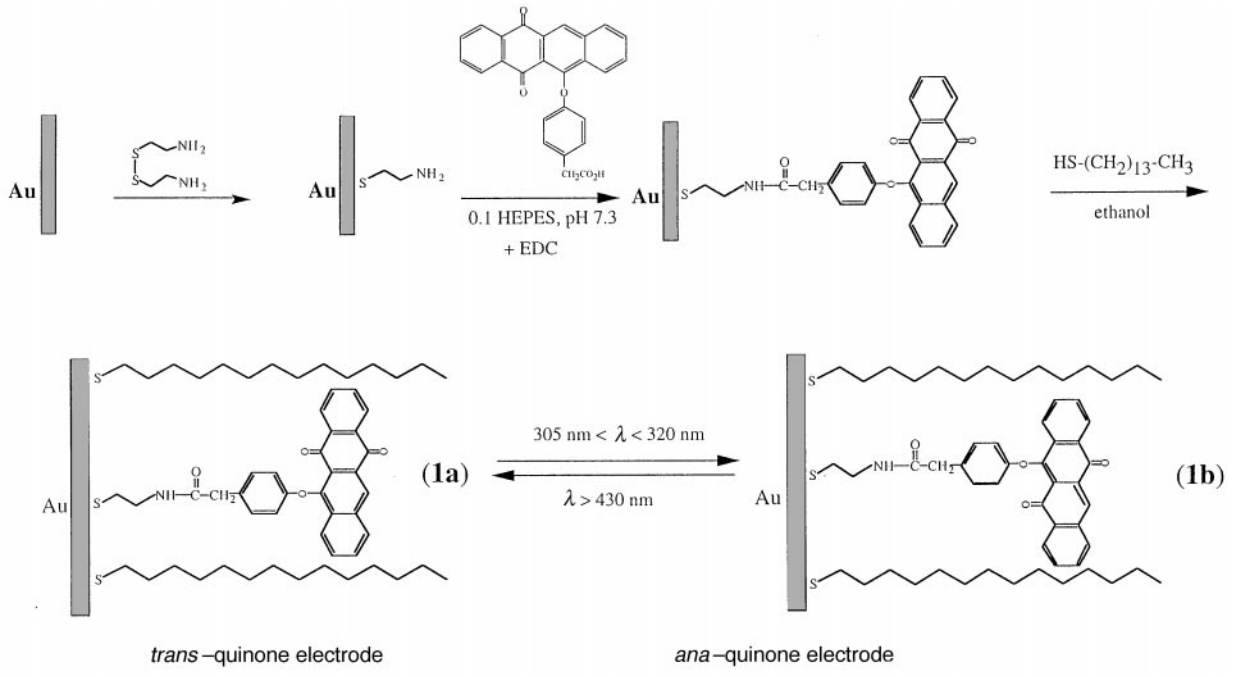

Scheme 1 Assembly of the phenoxynaphthacenequinone/C_{14}SH mixed monolayer on a Au electrode and its photoisomerization.

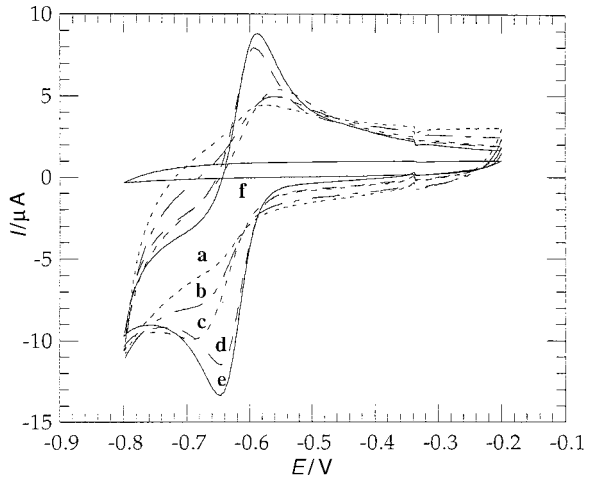

Fig. 3 Cyclic voltammograms of the *trans*-quinone monolayer electrode at different time intervals of treatment with long-alkyl mercaptan C_{14}SH (1 mM in ethanol): (a) before treatment, (b) 1, (c) 4, (d) 10, and (e) 30 min of treatment, respectively and (f) cyclic voltammogram of a Au electrode modified with C_{14}SH only (1 mM, 30 min). Electrolyte composition 0.01 M phosphate buffer, pH 7.0, and 0.1 Na_2SO_4; potential scan rate, 50 mV s^{-1}.

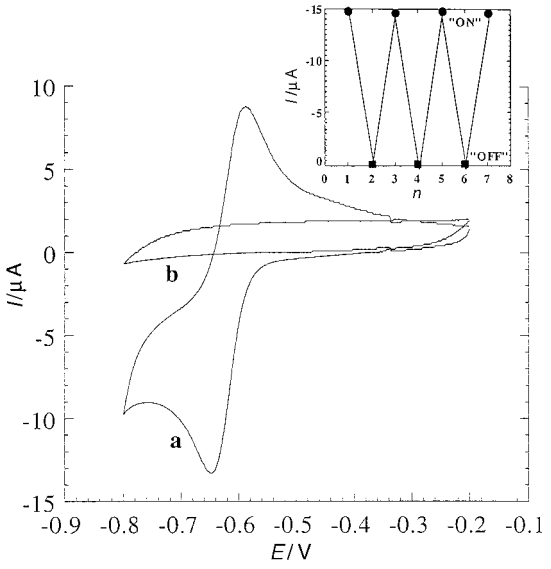

Fig. 4 Cyclic voltammograms of the photoisomerizable quinone/C_{14}SH mixed-monolayer electrode in the different isomeric states: (a) *trans*-quinone (**1a**) produced by irradiation, $\lambda > 430$ nm; (b) ana-quinone state (**1b**) formed by illumination, $305 < \lambda > 320$ nm. Electrolyte composition 0.01 M phosphate buffer, pH 7.0, 0.1 M Na_2SO_4, scan rate 50 mV s^{-1}. Inset: Cyclic amperometric transduction upon photoisomerization of the monolayer electrode (●) in the **1a** state, and (■) in the **1b**-state.

transduction of the recorded photonic signal. The amplification of photonic signals recorded by the phenoxynaphthacenequinone monolayer will be addressed here by the application of *N,N′*-dibenzyl-4,4′-bipyridinium, BV^{2+}, as a secondary electron relay. The reduction potential of BV^{2+} is pH-independent, and corresponds to −0.58 V (*vs.* SCE), where the formal reduction potential of the *trans*-quinone component at pH 7.5 is $E^\circ = -0.65$ V. This allows the vectorial reduction of BV^{2+} by the electroactive *trans*-quinone monolayer, and the activation of the respective electron transfer cascade. Fig. 5 shows the cyclic voltammograms of the photoisomerizable *trans*-quinone monolayer electrode in the absence (curve a) and presence (curve b) of BV^{2+}. With the relay unit, BV^{2+}, an electrocatalytic cathodic current is observed, indicating the vectorial electrocatalyzed reduction of the relay by the *trans*-hydroquinone component. Also, it is evident that the transduced current is *ca.* 10-fold enhanced in the presence of the electron relay. Photoisomerization of the monolayer to the 'ana'-quinone state, $305 < \lambda < 320$ nm, in the presence of BV^{2+} results in only the background current (curve c), implying that the direct electron transfer to BV^{2+} is prohibited. By cyclic photoisomerization of the monolayer between the *trans*-quinone and 'ana'-quinone states, the reversible amplified amperometric transduction of the recorded optical signals is observed.

The reduction potential of the *trans*-quinone monolayer is controlled by the pH of the electrolyte and is positively shifted as the pH decreases. For example, the formal potential of the *trans*-quinone monolayer corresponds to $E^\circ = -0.65$ V and $E^\circ = -0.51$ V (*vs.* SCE) at pH 7.5 and 5.0, respectively. This

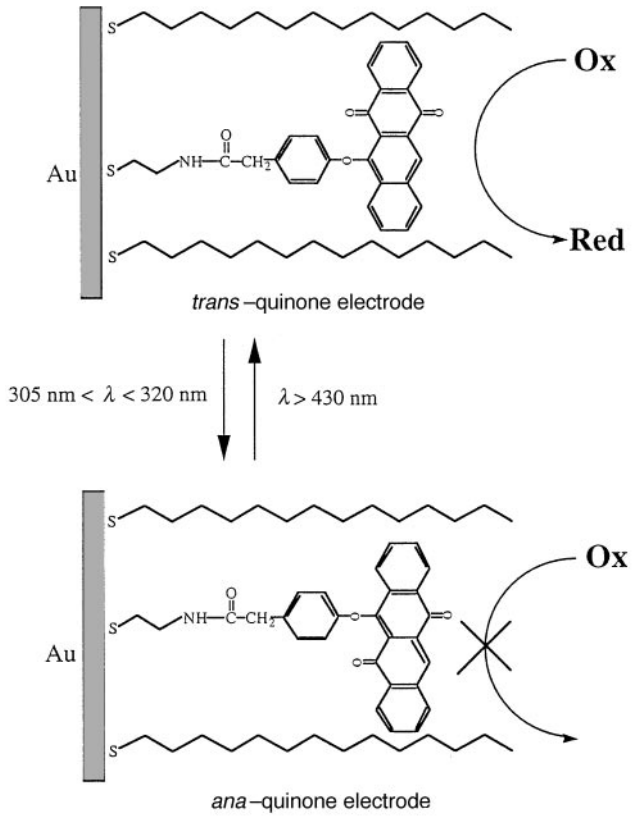

Scheme 2 Photoswitchable electrocatalytic reduction of an electron acceptor at the phenoxynaphthacenequinone/C_{14}SH mixed monolayer electrode interface.

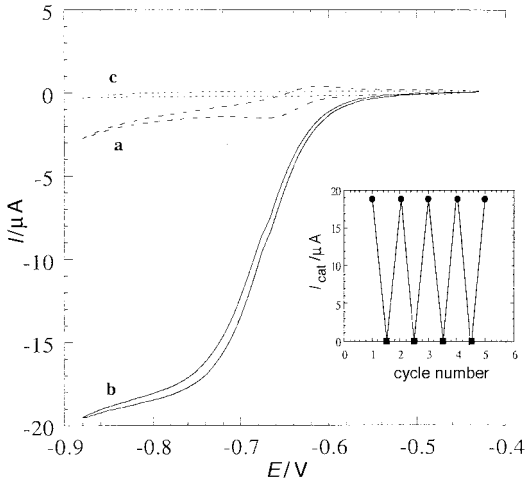

Fig. 5 Cyclic voltammograms of the quinone photoisomerizable/C_{14}SH monolayer electrode: (a) electrode in *trans*-quinone **1a** state in pure electrolyte solution; (b) electrode in *trans*-quinone **1a** state with benzyl viologen (BV^{2+}), 1×10^{-3} M, in electrolyte solution; (c) electrode in 'ana'-quinone **1b** state with BV^{2+}, 1×10^{-3} M in the electrolyte solution. Electrolyte composition as in Fig. 4, scan rate 5 mV s^{-1}. Inset: Cyclic amplified amperometric transduction of reversible photoactivated isomerization of the monolayer: (●) **1a** monolayer state; (■) **1b** monolayer state.

allows the control of the interfacial electron transfer features of the functionalized monolayer electrodes by external photonic and pH signals. At pH 5.0 the *trans*-quinone monolayer is thermodynamically prohibited from stimulating the electron transfer to BV^{2+} ($E^{\circ} = -0.58$ V). Only the weak electrical response of the *trans*-quinone monolayer is observed, without the activation of the electron transfer cascade. Thus, the phenoxynaphthacenequinone-functionalized monolayer electrode acts in the presence of BV^{2+} as a gated molecular optoelectronic system, duplicating the function of an 'AND' gate in an electronic circuit (Fig. 6). In the 'ana'-quinone state at pH 5.0, the system is in a mute configuration. Photoisomerization of the monolayer to the *trans*-quinone state does not yield the amplified amperometric response, since the electron transfer cascade that reduces BV^{2+} is not activated. Photoisomerization of the monolayer to the *trans*-quinone state, and alteration of the pH of the system to pH $\geqslant$ 7.5 facilitates the mediated electrocatalyzed reduction of BV^{2+} and the transduction of the amplified electronic current signal.

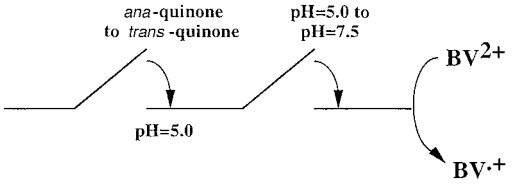

Fig. 6 Photochemical and pH-controlled reduction of benzyl viologen (BV^{2+}) by the **1a** monolayer electrode. An 'AND' molecular electronic gate.

Photoisomerizable monolayer electrodes controlling interfacial electron transfer

Photoisomerizable monolayers associated with conductive surfaces can act as active interfaces for controlling electron transfer at the electrode–solution interface [Fig. 2(b)]. The associative interactions between one photoisomer state of the monolayer and the redox probe present in the electrolyte lead to the formation of a complex between the electroactive substrate and the monolayer. Concentration of the redox probe at the functionalized support electrically contacts the substrate and the electrode and stimulates interfacial electron transfer. Various interactions, such as electrostatic, host–guest or donor–acceptor interactions, could yield the affinity binding of the redox probe to the photoisomerizable monolayer.

Charged monolayers were employed as active interfaces for controlling specific electron transfer at electrode supports.[40] Negatively charged monolayers associated with electrodes were used to discriminate the electrochemical reactions of a mixture of positively and negatively charged substrates.[41] Accordingly, we have designed a photoisomerizable monolayer on a Au electrode that alters the electrical charge on the conductive support.[42] 1-(4-Mercaptobutyl)-3,3-dimethyl-6′-nitrospiro[2′*H*-1-benzopyran-2′,2-indoline], mercaptobutylnitrospiropyran **2a**, was assembled on a Au electrode (Scheme 3). The nitrospiropyran monolayer SP state is neutral. Photoisomerization of the monolayer, 320 $< \lambda <$ 350 nm, yields at pH 7.0 the protonated nitromerocyanine (**2b**) monolayer MRH^{+} state. The latter monolayer is positively charged and thus the electrochemistry of charged redox substrates could be discriminated. Positively charged redox probes will be repelled by the functionalized electrode, where negatively charged species are attracted by the monolayer and enhance the electron transfer at the electrode surface (Scheme 4). The photostimulated oxidation of the negatively charged substrate, 3,4-dihydroxyphenylacetic acid at pH 7.0, DHPAA (**3**), and the positively charged substrate 3-hydroxytyramine (dopamine), DOPA (**4**) (at pH 7.0), was examined in the presence of the photoisomerizable monolayer electrode. Fig. 7(A) (curve a) shows the cyclic voltammogram corresponding to the electrochemical oxidation of DHPAA by the SP monolayer-functionalized electrode. Photoisomerization of the monolayer to the MRH^{+} monolayer state, 320 $< \lambda <$ 350 nm, results in the cyclic voltammogram shown in Fig. 7(A) (curve b). Regeneration of the SP monolayer by photoisomerization

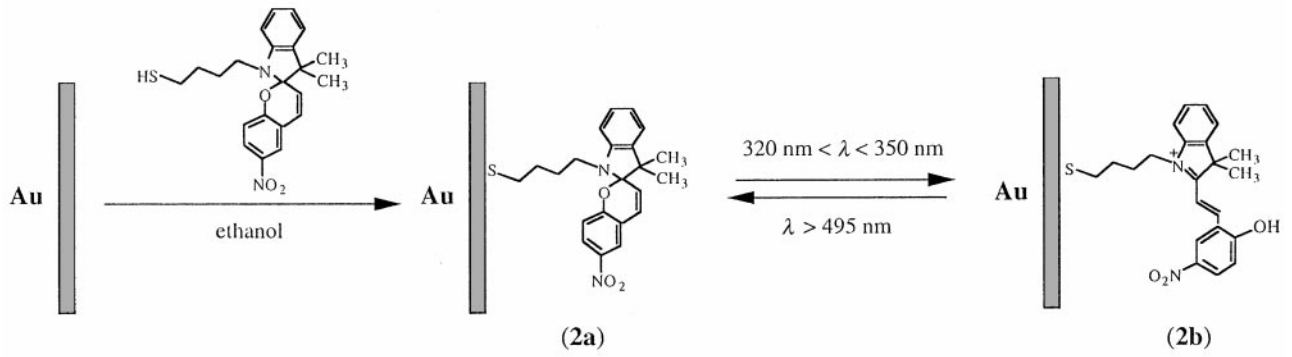

Scheme 3 Assembly of the nitrospiropyran monolayer on a Au electrode.

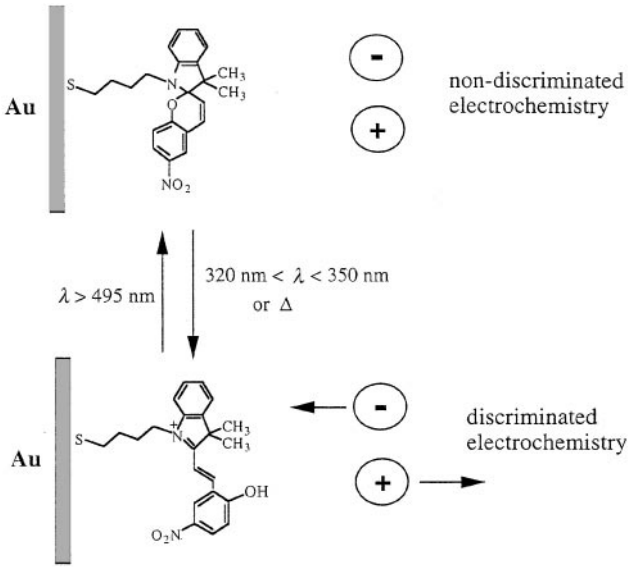

Scheme 4 Photochemically-controlled oxidation of DHPAA (**3**) and DOPA (**4**) at a nitrospiropyran-functionalized electrode.

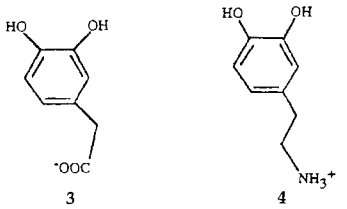

of the MRH^+ interface restores the cyclic voltammogram shown in curve c. By reversible photoisomerization of the monolayer between the SP and MRH^+ states, the amperometric responses of the electrode are cycled between low and high values, respectively [inset, Fig. 7(A)]. The high amperometric responses of the MRH^+ monolayer in the presence of DHPAA are attributed to the electrostatic attraction of the redox-active substrate to the positively charged monolayer interface. Concentration of DHPAA at the electrode surface facilitates electron transfer and results in high amperometric transduction of the attractive affinity interactions. With the positively-charged electroactive substrate DOPA, the direction of the transduced amperometric signals is reversed. Fig. 7(B) shows the cyclic voltammograms of DOPA in the presence of the photoisomerizable monolayer electrode. With the SP monolayer-functionalized electrode, a high amperometric response is observed (curve a). Photoisomerization of the monolayer to the protonated nitromerocyanine MRH^+ state retards the electrochemical oxidation of DOPA (curve b). Back photoisomerization of the MRH^+ monolayer to the SP state regenerates the high amperometric response of the electrode (curve c). By reversible photoisomerization of the monolayer between the SP and MRH^+ states, the amperometric responses of the electrode are cycled between high and low values, respectively [Fig. 7(B), inset]. Note that for DOPA, the high amperometric responses of the functionalized electrode are observed with the SP monolayer electrode. The retardation of the electrochemical oxidation of DOPA in the presence of the MRH^+ monolayer electrode is attributed to the electrostatic repulsion of DOPA by the positively charged interface.

Thus, the photoisomerization of the monolayer between the SP state and the protonated nitromerocyanine MRH^+ state provides a means to control the electrical features of the electrode surface, thereby regulating the electron transfer at the electrode interface. The SP monolayer results in a neutral electrode surface where the MRH^+ monolayer charges positively the surface and results in the formation of an electrical double-layer at the electrode interface.

Functionalized monolayer electrodes coupled to photoisomerizable substrates for the physical transduction of photonic signals

The assembly of monolayers on solid supports could lead to a functionalized interface that regulates the affinity interactions of a photoisomerizable substrate with the monolayer [Fig. 2(c)]. In one photoisomer state, the substrate associates to the functionalized monolayer, and concentration of the substrate at the solid support is physically transduced (*e.g.* an electrochemical, piezoelectric, impedance, surface plasmon resonance or ellipsometric, effect). In the complementary photoisomer state of the substrate, it lacks affinity for the monolayer, and the respective transduced signal is blocked. This approach for tailoring molecular optoelectronic assemblies was demonstrated by us, using different photoisomerizable substrates.[43,44] Two systems will be addressed here to exemplify the method. *trans*-*N*-Methyl-*N*′-(1-phenylazobenzyl)-4,4′-bipyridinium (**5t**) exhibits reversible photoisomerizable properties. Irradiation of **5t**, $\lambda = 355$ nm, yields the *cis*-isomer (**5c**), and further illumination of **5c**, $\lambda > 375$ nm, restores the *trans*-bipyridinium azobenzene substrate (**5t**). The two photoisomers differ substantially in their binding features to the β-cyclodextrin (β-CD) receptor. The association constants of **5t** and **5c** to β-CD are $K_a = 1700$ and $180\ M^{-1}$, respectively. Accordingly, amino-β-cyclodextrin (**6**) was synthesized and assembled on a Au electrode[43] (Scheme 5). The association of **5t** to the β-CD receptor monolayer is reflected by the high amperometric response of the electrode [Fig. 8 (curve a)]. Photoisomerization of the substrate to the *cis*-isomer state (**5c**) results in a substantially lower amperometric response [Fig. 8 (curve b)]. By cyclic photoisomerization of the substrate between the states **5t** and **5c**, reversible high and low current signals are transduced by the β-CD-functionalized electrode, respectively

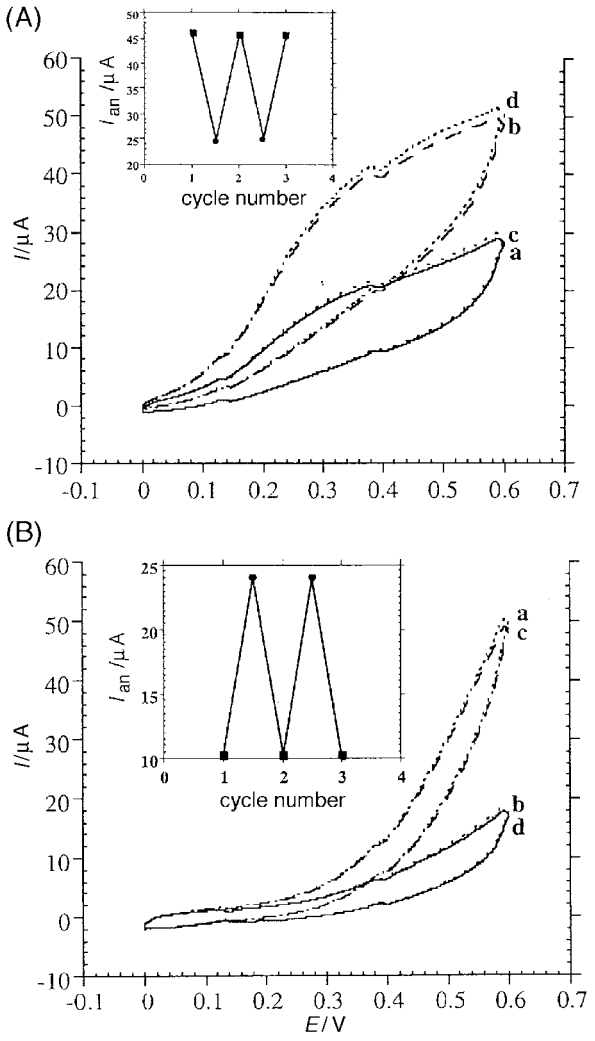

Fig. 7 Cyclic voltammograms of the nitrospiropyran **2** photoisomerizable electrode in the presence of charged electroactive substrates: (A) in the presence of DHPAA (5×10^{-4} M). Curves (a) and (c)—monolayer electrode in the nitrospiropyran state (**2a**). Curves (b) and (d)—monolayer electrode in the protonated merocyanine state (**2b**). Inset: Cyclic amperometric transduction upon reversible photoisomerization of the monolayer between the nitrospiropyran (**2a**) (●) and protonated merocyanine (**2b**) (■) states. (B) In the presence of DOPA (1×10^{-4} M). Curves (a) and (c)—monolayer electrode in the nitrospiropyran state (**2a**). Curves (b) and (d)—monolayer electrode in the protonated merocyanine state (**2b**). Inset: Cyclic amperometric transduction upon photoisomerization of the monolayer electrode between the nitrospiropyran state (**2a**) (●) and protonated merocyanine state (**2b**) (■). For all experiments, electrolyte compsoition 0.02 M phosphate buffer, pH 7.0. Potential scan rate 200 mV s^{-1}. Nitrospiropyran monolayer state (**2a**) was generated by irradiation, $\lambda>495$ nm. Protonated merocyanine monolayer state (**2b**) was formed by illumination $320<\lambda<350$ nm.

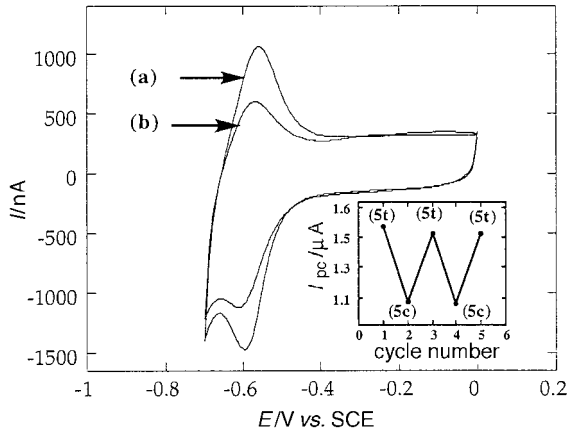

Fig. 8 Cyclic voltammograms at the cyclodextrin-functionalized Au electrode of (a) [**5t**] $=1\times10^{-6}$ M and (b) [**5c**] $=1\times10^{-6}$ M in 0.01 M phosphate buffer, pH 10.8, scan rate 100 mV s^{-1}, $T=25$ °C. Inset: cyclic cathodic responses of the **6** monolayer electrode measured at 0.6 V upon reversible photoisomerization of the diad between **5t** and **5c**, respectively.

(Fig. 8, inset). The high amperometric response of the electrode in the presence of **5t** is attributed to the concentration of the substrate at the electrode surface by its binding to the cyclodextrin receptor. The association of **5t** to the receptor monolayer, and its surface confinement, is supported by the fact that the cathodic peak currents (or anodic peak currents) observed in the cyclic voltammogram relate linearly to the scan rate ($i_p\propto\nu$). It should be noted that *trans*-bipyridinium azobenzene substrate **5t** yields, upon photoisomerization to **5c**, a photostationary equilibrium that includes *ca.* 10% of **5t**. Thus, it was estimated that *ca.* 40% of the current observed in the presence of **5c** originates from the residual **5t** that is present in the system as a result of the photostationary equilibrium.

Light-controlled formation and dissociation of donor–acceptor complexes at solid supports provides an alternative route for the physical transduction of optical signals. The formation of donor–acceptor complexes between bipyridinium salts (electron acceptors) and xanthene dyes (electron donors) (*e.g.* eosin, Rose Bengal) was extensively characterized in our laboratory.[45] We have identified the crystal structure of these complexes and characterized the structural features of the donor–acceptor complexes in solutions using NMR spectroscopy. We reported that the xanthene dye–bipyridinium donor–acceptor complexes are stabilized by charge-transfer interactions, π–π overlap, and attractive electrostatic interactions between the electron donor and electron acceptor units.[46] It was also demonstrated that the complexation features of photoisomerizable bipyridinium and bis-pyridinium electron acceptors to the xanthene dye are controlled by the photoisomer state of the electron acceptor.[14,44b] The formation and the dissociation of the supramolecular donor–acceptor complex between the xanthene dye and the bipyridinium unit could be triggered by the light-induced transformation of the latter component to photoisomers exhibiting high or low affinities for the electron donor, respectively. In these systems, reversible photoisomerization of the electron acceptor led to cyclic photoswitchable formation or dissociation of the respective donor–acceptor complexes in solution.

From the different systems that were developed in our laboratory,[44] the organization of a molecular optoelectronic system based on the eosin, Eo^{2-} (**7**), electron donor and the *trans*- or *cis*-3,3′-bis(*N*-methylpyridinium) azobenzenes **8t** or **8c** will be addressed.[44c] Fig. 9(A) shows the spectral changes of the eosin chromophore upon addition of *trans*-3,3′-bis(*N*-methylpyridinium) azobenzene **8t**. The absorbance maximum of the Eo^{2-} chromophore decreases, and from the spectral changes of Eo^{2-} at different concentrations of **8t** the association constant of the donor–acceptor complex was derived ($K_a=7.8\times10^4$ M^{-1}). Fig. 9(B) shows the spectral changes of the eosin chromophore upon addition of *cis*-3,3′-bis(*N*-methylpyridinium) azobenzene **8c**, electron acceptor. The latter is obtained upon photoisomerization of **8t**, $\lambda=355$ nm. Photoisomerization of **8t** to **8c** yields a photostationary state, where *ca.* 15% of **8t** is in equilibrium with **8c**. From the spectral changes of the Eo^{2-} upon addition of **8c**, and knowing the composition of the photostationary equilibrium, the association constant of the donor–acceptor complex between Eo^{2-} and **8c** was derived ($K_a=1.4\times10^4$ M^{-1}).

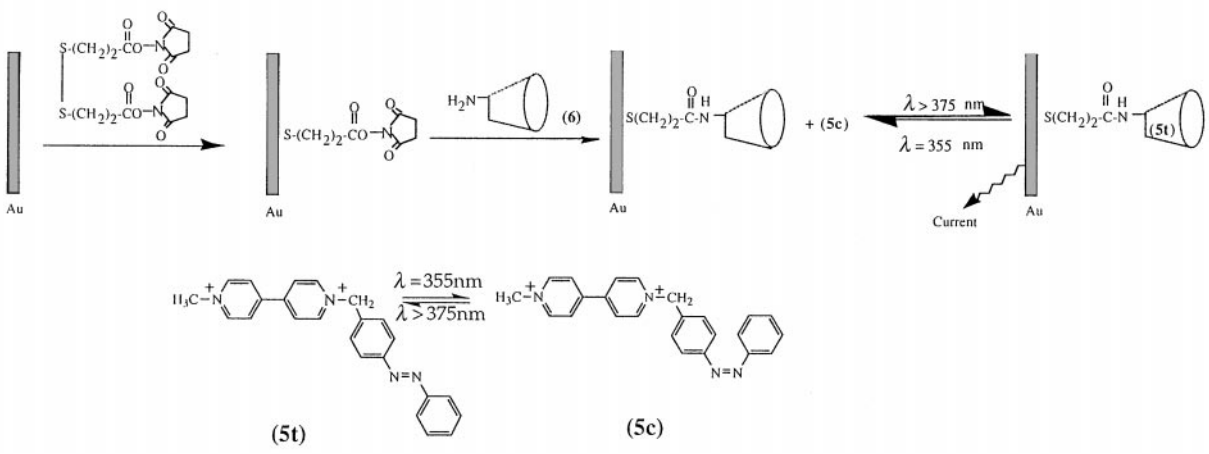

Scheme 5 Assembly of the amino-functionalized β-cyclodextrin (**6**) monolayer onto a Au surface.

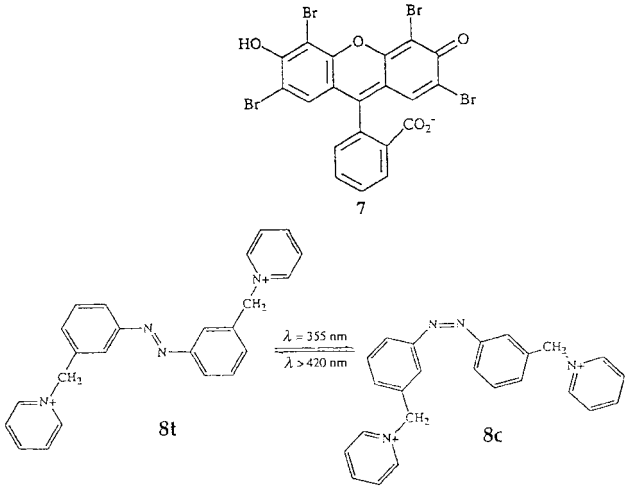

The high affinity of **8t** to the eosin chromophore, and the formation of the resulting donor–acceptor complex, is reflected by an absorbance decrease at $\lambda = 520$ nm. With **8c** the decrease is substantially lower. Thus, the system includes an internal optical transduction signal (absorbance) for the photoswitchable formation or dissociation of the donor–acceptor complex. Fig. 10 shows the cyclic absorbance changes of the eosin chromophore upon reversible photoisomerization of the electron acceptor between the states **8c** and **8t**. In the presence of **8c** the system reveals a high absorbance (OD = 0.65) while in the presence of **8t** the eosin absorbance is quenched (OD = 0.35), indicating the formation of the supramolecular donor–acceptor complex between eosin and **8t**. By photoisomerization of the electron acceptor between the states **8t** and **8c**, the reversible photostimulated formation of the donor–acceptor complex and its dissociation are observed, respectively.

Tailoring of molecular optoelectronic systems based on the photoswitchable complexation features of Eo^{2-} and **8t** or **8c** requires the integration of the molecular components with a transducing support to the extent that the light-stimulated formation and dissociation of the respective donor–acceptor complexes are electronically transduced. Since the electron acceptors **8t** or **8c** are electrochemically inactive, the amperometric detection of the formation or dissociation of the complexes at electrode surfaces is impossible. To overcome this difficulty, we have applied the piezoelectric phenomenon and the microgravimetric detection of the formation and dissociation of the donor–acceptor complexes at a piezoelectric crystal as an electronic transduction means.[44c] For a piezoelectric quartz crystal, the change in resonance frequency (Δf) upon a mass change (Δm) occurring on the crystal is given by

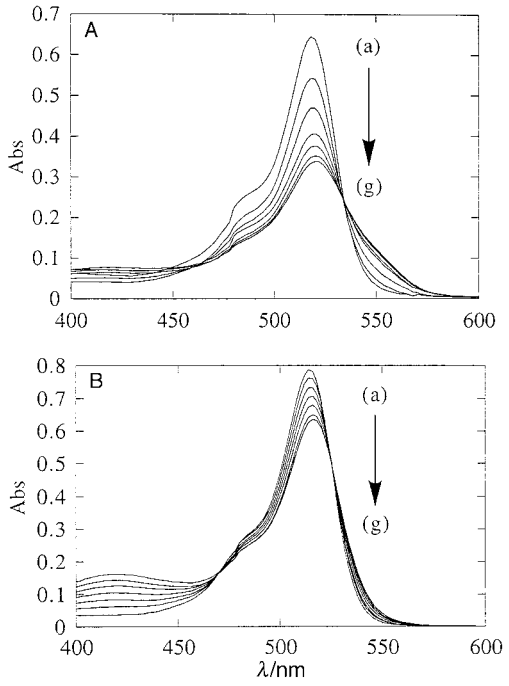

Fig. 9 (A) Spectral changes of an aqueous solution of eosin (1×10^{-5} M), at different concentrations of added **8t** corresponding to: (a) 0, (b) 6.6×10^{-6}, (c) 1.32×10^{-5}, (d) 1.96×10^{-5}, (e) 2.6×10^{-5}, (f) 3.2×10^{-5} and (g) 3.85×10^{-5} M. (B) Spectral changes of an aqueous solution of eosin (1×10^{-5} M) at different concentrations of **8c** corresponding to (a) 0, (b) 6.6×10^{-6}, (c) 1.32×10^{-5}, (d) 1.96×10^{-5}, (e) 2.6×10^{-5}, (f) 3.2×10^{-5} and (g) 3.85×10^{-5} M.

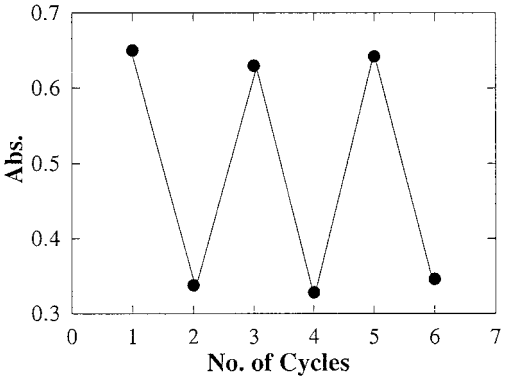

Fig. 10 Reversible spectroscopic transduction of light-stimulated dissociation and association of the photoisomerizable electron acceptors **8c** and **8t** to eosin. $[Eo^{2-}] = 1 \times 10^{-5}$ M, [**8t**] $= 3.8 \times 10^{-5}$ M.

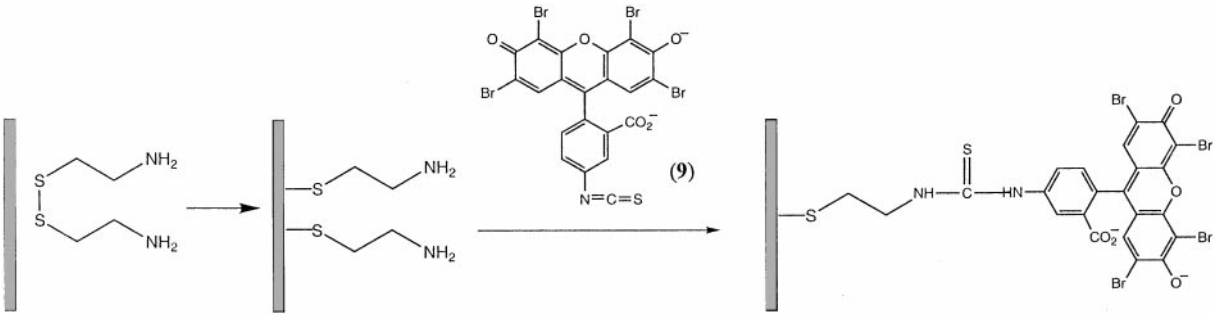

Scheme 6 Assembly of an eosin monolayer on Au electrodes associated with a quartz crystal.

the Sauerbrey equation [eqn. (1)]. In this relation, f_o is the basic frequency of the crystal, ρ_q is the quartz density, m_q is the

$$\Delta f = -\left[\frac{2nf_o^2}{(\rho_q m_q)^{1/2}}\right]\Delta m = -\left(\frac{f_o^2}{N\rho_q}\right)\Delta m = -C_f\Delta m \qquad (1)$$

shear-modulus of the crystal, and n is the wave number. Thus, an increase in the crystal mass by Δm is associated with a decrease of the crystal resonance frequency by $-\Delta f/C_f$ Hz. Similarly, a decrease in the crystal mass will be reflected by an increase in the crystal frequency. For piezoelectric quartz crystals, AT-cut, exhibiting the characteristic resonance frequency of $f_o = 9\times10^6$ Hz, the value C_f corresponds to 2.66×10^8 Hz cm.

The eosin electron donor was assembled on Au electrodes associated with a quartz crystal by the coupling of eosin isothiocyanate (**9**) to a cystamine monolayer linked to the Au surfaces, Scheme 6. The linkage of the eosin component to the base cystamine monolayer is associated with a decrease of the crystal frequency that corresponds to $\Delta f = -300$ Hz. This value translates to an eosin coverage that corresponds to 1.6×10^{-9} mol cm^{-2} on the Au surface. Fig. 11(A) shows the crystal frequency changes upon interaction of the eosin-functionalized Au-quartz crystal with different concentrations of **8t**. As the bulk concentration of **8t** is elevated, the decrease in the crystal frequency is enhanced, indicating that the association of the electron acceptor to the monolayer increased. For each bulk concentration of **8t**, the crystal frequency levels off

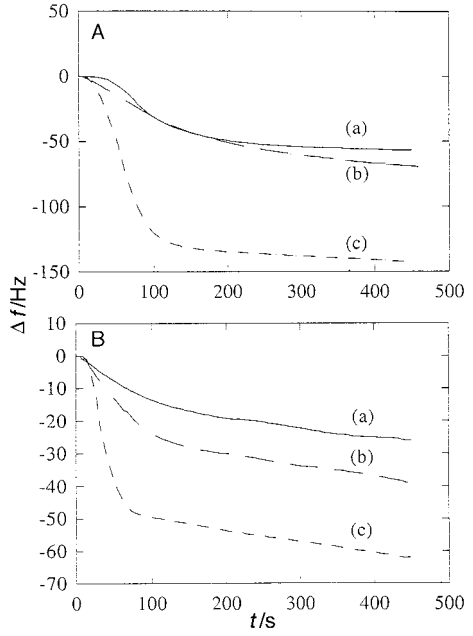

Fig. 11 Frequency changes of the eosin-modified quartz crystal upon interaction with different concentrations of (A) [**8t**] corresponding to (a) 1.47×10^{-4}, (b) 2.20×10^{-4} and (c) 2.94×10^{-4} M; (B) [**8c**] corresponding to (a) 7.35×10^{-5}, (b) 1.47×10^{-4} and (c) 2.2×10^{-4} M.

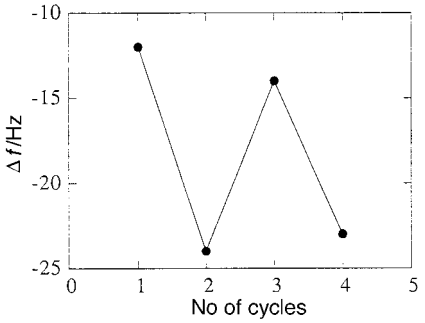

Fig. 12 Cyclic frequency changes of the eosin-modified quartz crystal upon photoisomerization of the electron acceptor between states **8t** and **8c**. All experiments were performed in an aqueous solution, [**8t**] = [**8c**] = 7.35×10^{-5} M. Frequencies were determined 10 min after interaction between the functionalized crystal and the respective isomer state of the electron acceptor.

to a new decreased constant frequency that relates to the equilibrium coverage of the monolayer by **8t**. Fig. 11(B) shows the crystal frequency changes upon challenging the eosin monolayer with different concentrations of **8c**. Note that for the **8c** electron acceptor, the decrease of the crystal frequency is substantially lower as compared to the identical system with the **8t** isomer. This implies that **8c** exhibits a lower binding affinity to the eosin monolayer as compared to the **8t** photoisomer state. Fig. 12 shows the cyclic microgravimetric, QCM transduction of the photostimulated binding of **8t** to the eosin monolayer and the dissociation of the complex at the crystal interface upon photoisomerization of the electron acceptor to **8c**. With **8c**, a frequency decrease of *ca.* $\Delta f = -(12\pm3)$ Hz is observed. Photoisomerization of the electron acceptor to the **8t** state results in the decrease of the crystal frequency $\Delta f = -(25\pm3)$ Hz, implying the binding of the electron acceptor to the monolayer assembly. Further isomerization of the electron acceptor to the **8c** state yields the original frequency decrease characteristic for this photoisomer, indicating the release and dissociation of **8c** from the monolayer interface. Using eqn. (1) and the observed frequency changes in the presence of **8t** and **8c** we estimate the surface coverage of the monolayer to be 2.9×10^{-10} and 1.4×10^{-10} mol cm^{-2} by the two electron acceptors, respectively.

Molecular optoelectronic machines

The previous sections addressed different methods to organize molecular optoelectronic systems based on the use of a light-active compound that is present in one of two photoisomer states. The interactions of these photoisomers with the electrode or functionalized electrode interfaces were electronically transduced and yielded the integrated molecular optoelectronic systems. One could, however, envisage more complex assemblies duplicating the functions of macroscopic machines and acting as molecular optoelectronic system, (MOSs).

Macroscopic machines include several basic features that can be adopted in tailoring of MOSs: (i) The machine is triggered by an external signal to the 'ON' and 'OFF'-states, *e.g.* an electrical or photonic signal. (ii) The activated machine performs a dynamic process, *e.g.* rotation or translocation. (iii) Usually, the machine exhibits the ability to transduce its position and its phase of activity.

Chemistry has reached high levels of molecular architecture, ingenious synthesis and molecular assemblage. It is, however, a future scientific challenge to organize 'molecular machines'. This goal involves the immobilization of molecular systems on a transducer interface. External signals trigger the movement, translocation or structural perturbation between distinct molecular states that are recognized, identified and transduced by the transducer element.

We have shown that chronoamperometric kinetic resolution of the electron transfer rates to or from a redox-active monolayer, associated with an electrode, provides a sensitive means to characterize the composition and configuration of the electroactive monolayer.[47] For a single kind of redox-active monolayer associated with an electrode, the current transient upon the application of a reductive (or oxidative) potential step follows an exponential decay with a time constant that corresponds to the interfacial electron-transfer rate constant. For two very similar redox species in the monolayer array that differ slightly in their chemical structure or position, the current transient upon the application of the potential step is expected to follow a biexponential decay [eqn. (2)], where k_1 and k_2 and Q_1 and Q_2 are the interfacial electron transfer rates, and the monolayer coverage of the two redox-active species, respectively. For example,

$$I(t)=(Q_1k_1)e^{-k_1t}+(Q_2k_2)e^{-k_2t} \quad (2)$$

N,N′-bis(carboxyalkyl)-4,4′-bipyridinium (**10**) was coupled to a base cystamine monolayer linked to a Au electrode, Scheme 7. The synthesis of the monolayer yields two modes of attachment of the bipyridinium salt to the monolayer. One mode includes the one-point attachment of the redox-active unit to the monolayer, while the second mode involves the two-point, bridged, linkage of the electron acceptor to the electrode. The two bipyridinium salt configurations exhibit similar redox potentials, and thus cannot be resolved by the pulsed voltammetric method. The electron transfer rates to the two electron-acceptor configurations differ sufficiently and enable the kinetic resolution of the electron transfer by chronoamperometry. Fig. 13 shows the chronoamperometric response of the generated monolayer. The current decay follows biexponential kinetics, consistent with two electron transfer rates to the different populations of the electron acceptor configurations [eqn. (2)]. The faster rate constant, $k_1=900\pm30\ s^{-1}$, is attributed to electron transfer to two-point-attached bipyridinium salt, while the slower rate constant, $k_2=500\pm30\ s^{-1}$, corresponds to the electron transfer to one-point attached bipyridinium salt. This explanation was supported by the selective production of single-point and two-point monolayer-linked bipyridinium relay units using a high concentration or a low concentration of the bipyridinium salt in the modification procedure, respectively. These experimental

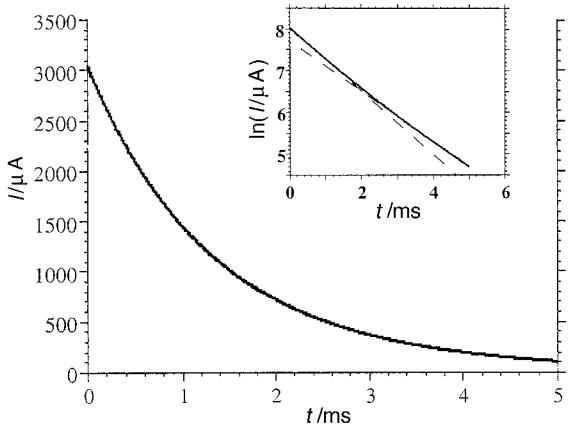

Fig. 13 Current response of the Au electrode modified with *N,N′*-bis(7-carboxyheptyl)-4,4′-bipyridinium monolayer rigidified with $C_{14}SH$ following a potential step from −0.3 to −0.69 V. Electrolyte composition 0.1 M phosphate buffer, pH 7.0. Inset: semilogarithmic plot for the current response.

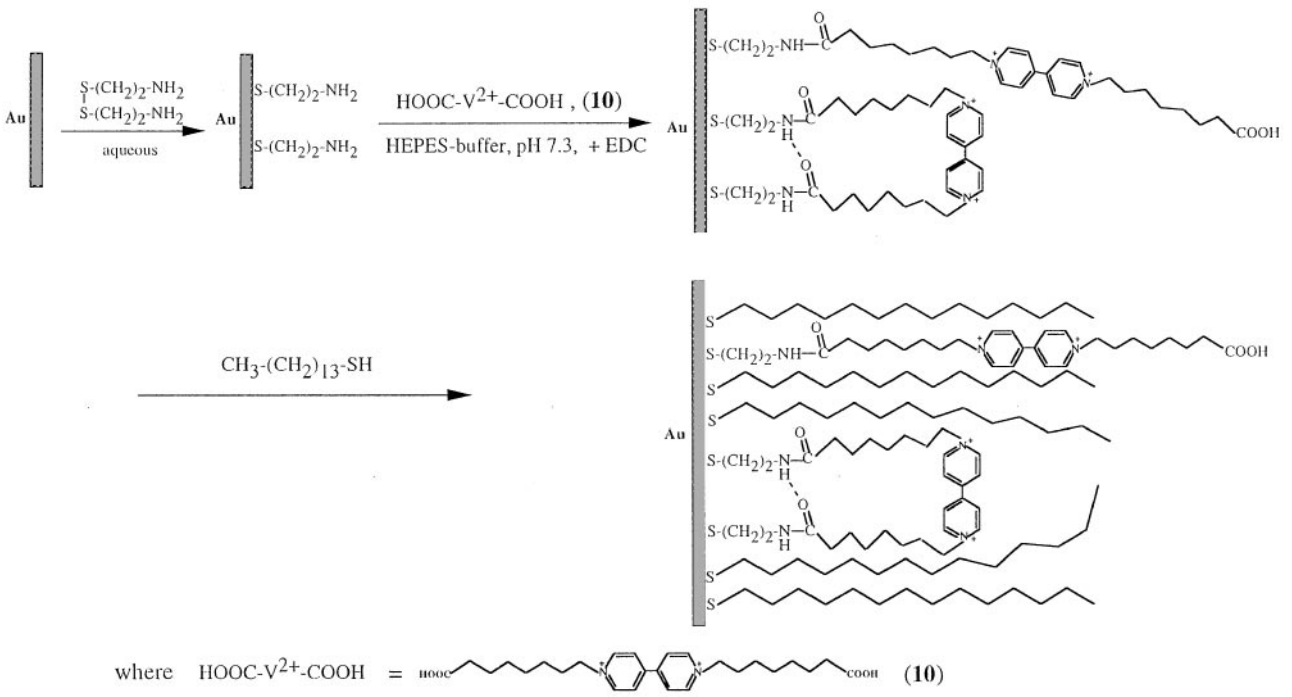

Scheme 7 Assembly of *N,N′*-bis(7-carboxyheptyl)-4,4′-bipyridinium as a monolayer *via* single- and double-point coupling to a cystamine-modified Au electrode.

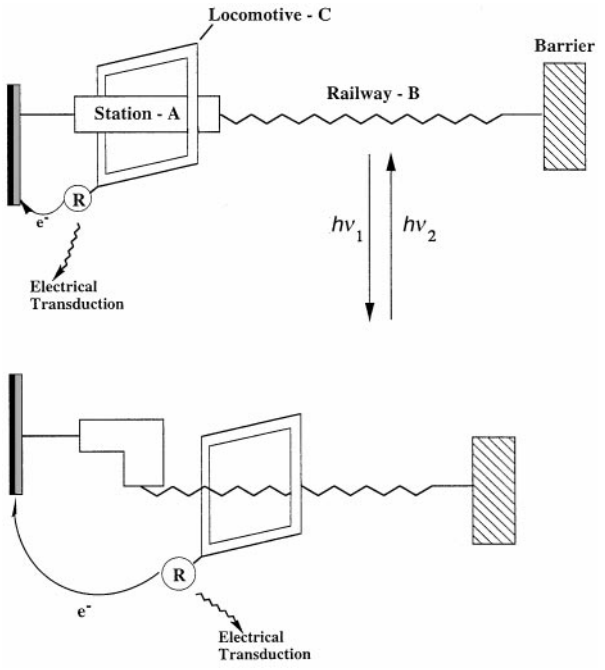

Scheme 8 Assembly of a nanoscale molecular assembly acting as a light-stimulated 'molecular-train'.

conditions favor the single-point and two-point linkage modes, respectively, and accordingly led to the faster and slower single exponential electron transfer rates of the resulting monolayers. This approach of kinetic resolution of electron transfer rates at redox-active monolayers was applied to characterize various electroactive composite monolayers. As the electron transfer rate is sensitive to the position of the redox-active component with respect to the electrode surface, any structural change or translocation of the electroactive unit is anticipated to be reflected by the interfacial electron transfer rate. In general, increasing the distance between the redox-active unit and the electrode surface retards the electron-transfer rate. Thus, the chronoamperometric response of a signal-translocated electroactive component on a molecular network is anticipated to transduce its steric position in the assembly.

The molecular optoelectronic system mimicking functions of a molecular machine is schematically described in Scheme 8, where a light-activated 'molecular train' is assembled on an electrode.[48] The assembly consists of a 'station', A, and a 'railway', B, linked to the conductive support. The molecular component, 'C', acting as the 'locomotive' is threaded onto the 'railway-station' assembly and protected by a barrier ('stopper') from dissociation. The preferred 'locomotive' position is at the station due to affinity interactions. Photoisomerization of the station to a state that lacks affinity for the 'locomotive' component results in its translocation to the 'railway' position. Back photoisomerization of the station unit to its original state restores the high-affinity site for the 'locomotive' and regenerates the primary state of the moveable molecular assembly. Provided the threaded molecular shuttle is redox-active, then its chronoamperometric response provides a means for the transduction of the 'locomotive' position on the molecular 'railway-station' wire.

The molecular shuttle or 'locomotive' is ferrocenylcarboxamide–β-cyclodextrin, Fc–β-CD (**11**). This substrate includes the β-cyclodextrin receptor site and the redox-active ferrocene label. Scheme 9 shows the assembly of the 'molecular train'. 4,4′-Dicarboxy-*trans*-azobenzene was covalently coupled to a cystamine monolayer associated with a Au electrode. 1,12-Diaminododecane was then linked to the azobenzene unit. The *trans*-azobenzene alkyl chain molecular wire monolayer includes the *trans*-azobenzene site, exhibiting a high-affinity binding site for β-cyclodextrin, and the alkyl chain component of lower binding properties to β-cyclodextrin. In order to generate a single molecular shuttle on the 'railway-station' array, the *trans*-azobenzene site was photoisomerized to the *cis*-azobenzene state. The receptor Fc–β-CD was then threaded onto the alkyl-chain, and the supramolecular complex was

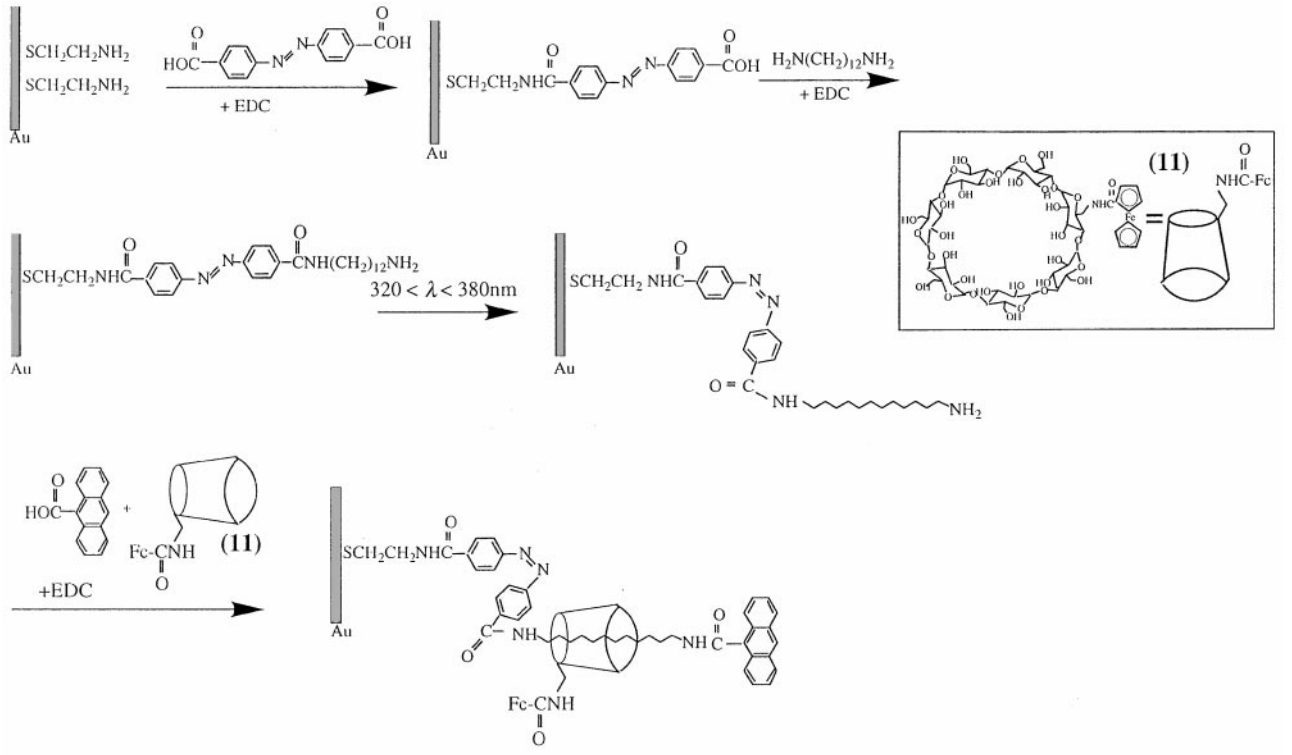

Scheme 9 Assembly of a monolayer consisting of ferrocene-functionalized β-cyclodextrin threaded onto an azobenzene-alkyl chain monolayer and blocked with an anthracene barrier on a Au electrode.

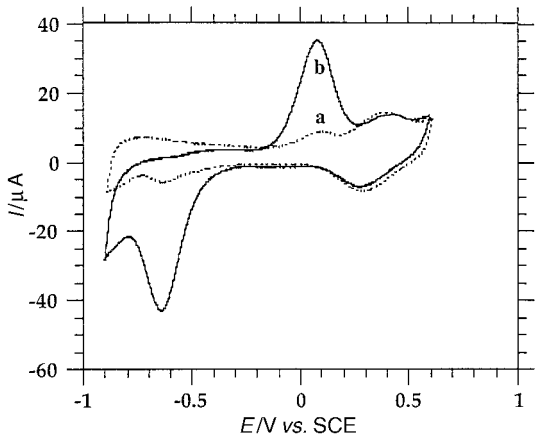

Fig. 14 Cyclic voltammograms of the assembly consisting of ferrocene-functionalized β-cyclodextrin threaded onto the azobenzene-alkyl chain and blocked by the anthracene barrier. (a) Monolayer in the *cis*-azobenzene configuration. (b) Monolayer in the *trans*-azobenzene configuration. Data recorded in 0.1 M phosphate buffer, pH 7.3. Scan rate 500 mV s^{-1}.

stoppered by coupling of anthracene-9-carboxylic acid to the amino function of the 'railway' element. The organization of the supramolecular monolayer assembly was confirmed by electrochemical means (Fig. 14). The cyclic voltammogram of the monolayer consists of the two-electron and two-proton reduction of the *trans*-azobenzene to hydrazobenzene (and the respective oxidation process), and the one-electron redox process of the ferrocene unit at $E^{\circ} = 0.31$ V *vs.* SCE of the threaded Fc–β-CD.

Scheme 10 shows schematically the light-induced translocation of the Fc–β-CD unit on the *trans*-azobenzene alkyl chain path, and the electrochemical transduction of the position of the 'molecular shuttle' in the system. In the *trans*-azobenzene state of the molecular wire, the 'locomotive', Fc–β-CD, is associated to the azobenzene 'station'. The close position of the redox label to the electrode surface is expected to yield a fast interfacial electron transfer. Photoisomerization of the *trans*-azobenzene unit to *cis*-azobenzene is expected to translocate Fc–β-CD to the alkyl chain, or 'railway position'. Spatial separation of the ferrocene redox label with respect to the electrode surface is anticipated to retard the interfacial electron transfer rate. Fig. 15(A) (curve a) shows the chronoamperometric response of the ferrocene–β-cyclodextrin

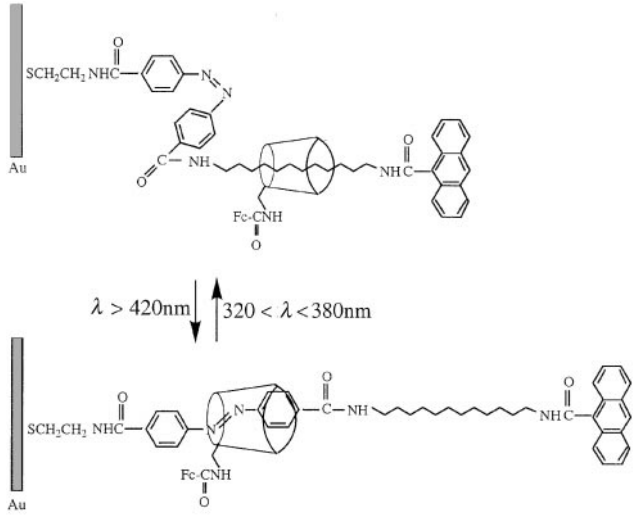

Scheme 10 Photoinduced translocation of ferrocene-functionalized β-cyclodextrin between the azobenzene-alkyl chain sites by cyclic light-induced isomerization of the monolayer.

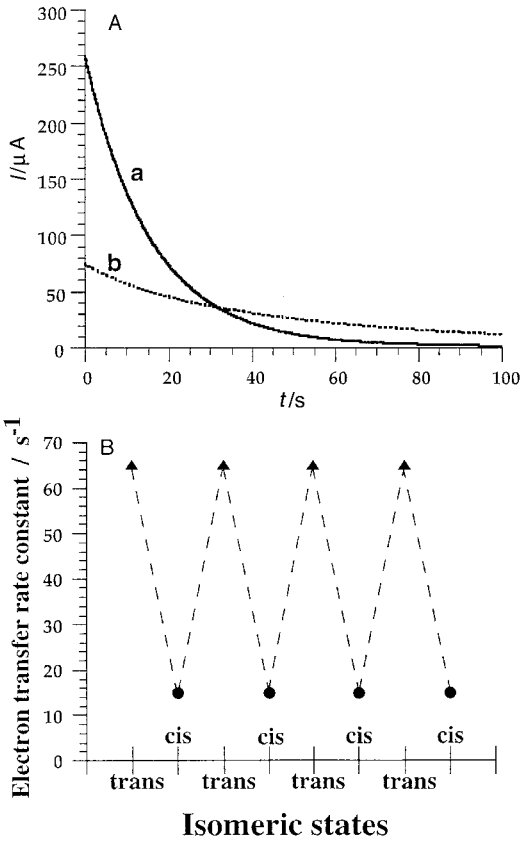

Fig. 15 (A) Chronoamperometric responses of the assembly consisting of the ferrocene-functionalized β-cyclodextrin threaded onto the azobenzene-alkyl chain and blocked by the anthracene barrier. (a) Monolayer in *trans*-azobenzene state. (b) Monolayer in *cis*-azobenzene state. (B) Cyclic variation of the electron transfer rates of the ferrocene-functionalized β-cyclodextrin in the molecular 'train-shuttle' upon reversible photoisomerization of the monolayer: (▲) monolayer in *trans*-azobenzene state, (●) monolayer in *cis*-azobenzene state.

in the presence of the *trans*-azobenzene monolayer assembly. A fast current decay, $k_{et}^{(1)} = 65\ s^{-1}$, is observed, implying that the molecular shuttle is close to the electrode surface. Photoisomerization of the monolayer to the *cis*-azobenzene configuration, $320 < \lambda < 380$ nm, results, for Fc–β-CD, in the chronoamperometric transient shown in Fig. 15(A), (curve b). A substantially lower electron transfer rate constant is observed ($k_{et}^{(2)} = 15\ s^{-1}$) indicating that the threaded receptor is positioned on the monolayer array in a spatially separated configuration with respect to the electrode surface. This is consistent with the translocation of the ferrocene–β-cyclodextrin from the *trans*-azobenzene 'station'-position to the alkyl chain 'railway' site. Further photoisomerization of the *cis*-azobenzene unit to the *trans*-azobenzene configuration, $\lambda > 420$ nm, restores the chronoamperometric response, characteristic for the receptor positioned on the *trans*-azobenzene unit. By cyclic photoisomerization of the monolayer between the *trans*-azobenzene and *cis*-azobenzene configurations, the threaded receptor is reversibly moved between the *trans*-azobenzene 'station' site and the alkyl chain 'railway' component [Fig. 15(B)]. The controlled light-stimulated dynamic translocation of the receptor between the two monolayer states is electronically transduced by the chronoamperometric response of the redox-labeled receptor.

Conclusions and perspectives

The present article summarizes our recent research activities in tailoring molecular optoelectronic assemblies where light

signals are recorded in the form of a chemical event on a monolayer assembly associated with a conductive support. The electronic transduction of the chemical feature stored in the monolayer provides a means to read the stored photonic information. The reversible photoisomerizable properties of the monolayer allow us to erase the stored information, and to reactivate the monolayer interface for the renewal of optical storage. Thus, the systems reveal 'Write-Read-Store' features.

To date, photoswitchable molecular assemblies have been tailored in the solution phase, and the state of the molecular switch was elucidated by spectroscopic assay, *e.g.* NMR analysis. Our scientific efforts are aimed to integrate the photoswitchable molecular features with a solid support that permits the electronic transduction of the photonic information. This is a desirable evolutionary step from solution photochemistry to an optoelectronic device. We have addressed two electronic transduction means of the stored optical information, *e.g.* amperometric and piezoelectric signaling. Other transduction signals, such as impedance, surface plasmon resonance (SPR) or ellipsometry, can be envisaged to follow the photoswitchable properties at the functionalized solid surface. We have followed several methods to design and tailor molecular optoelectronic systems. These included the organization of photochemically-triggered 'command surfaces' that control interfacial electron transfer, the functionalization of electrodes with receptor sites that control the association of photoisomerizable molecular species with the modified surface, and the assembly of photochemically redox-activated monolayer systems.

Finally, we have demonstrated that the concept of molecular optoelectronics can be expanded from static photoswitchable assemblies to dynamic photochemically-triggered molecular systems. This has been exemplified by the tailoring of a 'molecular train' that includes a 'station' and a 'railway', and a molecular 'locomotive' is translocated by light signals between the 'station-railway' sites. The molecular 'locomotive' electrically transduces its position on the molecular array. Such dynamic molecular assemblies, where light signals activate molecular motion that is transduced to the macroscopic environment, represent the first steps towards 'molecular machinery'. Based on our results, one could envisage more complex assemblies that include several 'stations' and a 'railway', complementary electro- and opto-activation of the molecular translocation, and application of intermediary photosensitizer sites as signaling sites for the dynamic processes.

The architecture of the molecular systems on the solid supports involved the assemblies of photoactive monolayers. The monolayer represents a two-dimensional array on the solid support. The rapid progress in the development of scanning nano-scale irradiation sources, *e.g.* scanning near-field optical microscope (SNOM), and the well-established scanning techniques to image a redox activated or conductive interface, *e.g.* by STM or scanning electrochemical microscopy, open the way to generate addressable optoelectronic nanostructures.

The future perspectives of this challenging project of molecular optoelectronics rests on the mandatory need for an interdisciplinary effort that combines chemistry, physics, electronics and material science.

The support of this study by The Israel Science Foundation founded by The Israel Academy for Science and Humanities, and by The Israel Ministry of Science (MOS) under the Infrastructure Project on Novel Materials and Functions, is gratefully acknowledged. Special thanks are directed to my coworkers who contributed their skills, enthusiasm and efforts to the success of the project. Their names appear in the reference list.

References

1 (*a*) J.-M. Lehn, *Angew. Chem.*, *Int. Ed. Engl.*, 1990, **102**, 1347; (*b*) F. L. Carter, A. Schultz and D. Duckworth, in *Molecular Electronic Devices*, ed. F. L. Carter, Marcel Dekker, New York, 1987, p. 183.
2 (*a*) V. Balzani, L. Moggi and F. Scandola, in *Supramolecular Photochemistry*, ed. V. Balzani, Reidel, Dordrecht, 1987, pp. 1–28; (*b*) *Molecular Electronic Devices*, ed. F. L. Carter, R. E. Siatkowsky and H. Woltjien, Elsevier, Amsterdam, 1988; (*c*) P. Ball, *Nature*, 1993, **362**, 123.
3 A. P. DeSilva, H. Q. N. Gunaratne and C. P. McCoy, *Nature*, 1993, **364**, 42.
4 P. Ball and L. Garwin, *Nature*, 1992, **355**, 761.
5 D. Bradley, *Science*, 1993, **259**, 890.
6 (*a*) R. A. Bissell, A. P. DeSilva, H. Q. N. Gunaratne, P. L. M. Lynch, G. E. M. Maguire, C. P. McCoy and K. R. A. S. Sandanayake, *Top. Curr. Chem.*, 1993, **168**, 223–264; (*b*) W. Göpel and P. Heiduschka, *Biosens. Bioelectron.,* 1995, **10**, 853.
7 (*a*) I. Willner, E. Katz and B. Willner, *Electroanalysis*, 1997, **9**, 965; (*b*) E. Katz, V. Heleg-Shabtai, B. Willner and I. Willner, *Bioelectrochem. Bioenerg.*, 1997, **42**, 95; (*c*) I. Willner, R. Blonder, E. Katz, A. Stocker and A. F. Bückmann, *J. Am. Chem. Soc.*, 1996, **118**, 5310.
8 K. E. Drexler, *Nanosystems*, *Molecular Machinery*, *Manufacturing and Computation*, Wiley, New York, 1992.
9 (*a*) G. De Santis, L. Fabbrizzi, M. Licchelli, M. Pallavicini, A. Perotti and A. Poggi, *Supramol. Chem.*, 1994, **3**, 115; (*b*) L. Fabbrizzi and A. Poggi, *Chem. Soc. Rev.*, 1995, **24**, 197.
10 (*a*) J. D. Winkler, K. Deshayes and B. Shao, in *Bioorganic Photochemistry–Biological Application of Photochemical Switches*, ed. H. Morrison, Wiley, New York, 1993, vol. 2, p. 169; (*b*) J. Rosengaus and I. Willner, *J. Phys. Org. Chem.* 1995, **8**, 54; (*c*) F. Würthner and J. Rebek, Jr., *Angew. Chem., Int. Ed. Engl.*, 1995, **34**, 446.
11 (*a*) S. Shinkai, T. Minami, T. Kusano and O. Manabe, *J. Am. Chem. Soc.* , 1982, **104**, 1967; (*b*) P. R. Ashton, R. Ballardini, V. Balzani, A. Credi, M. T. Gandolfi, S. Menzer, L. Pérez-García, L. Prodi, J. F. Stoddart, M. Venturi, A. J. P. White and D. J. Williams, *J. Am. Chem. Soc.*, 1995, **117**, 11171.
12 (*a*) S. L. Gilat, S. H. Kawai and J.-M. Lehn, *Chem. Eur. J.*, 1995, **1**, 275; (*b*) S. H. Kawai, S. L. Gilat, R. Ponsinet and J.-M. Lehn, *Chem. Eur. J.*, 1995, **1**, 285; (*c*) S. Liu, K. Hashimoto and A. Fujishima, *Nature*, 1990, **347**, 658; (*d*) K. Morigaki, Z. Liu, K. Hashimoto and A. Fujishima, *J. Phys. Chem.*, 1995, **99**, 14771.
13 R. Blonder, E. Katz, I. Willner, V. Wray and A. F. Bückmann, *J. Am. Chem. Soc.*, 1997, **119**, 11747.
14 I. Willner, S. Marx and Y. Eichen, *Angew. Chem.*, *Int. Ed. Engl.*, 1992, **31**, 1243.
15 (*a*) S. H. Kawai, S. L. Gilat and J.-M. Lehn, *J. Chem. Soc.*, *Chem. Commun.*, 1994, 1011; (*b*) L. Zelikovich, J. Libman and A. Shanzer, *Nature*, 1995, **374**, 790.
16 T. R. Kelly, M. C. Bowyer, K. V. Bashkar, D. Debbington, A. Garcia, F. Lang, M. H. Kim and M. P. Jette, *J. Am. Chem. Soc.*, 1994, **116**. 3657.
17 T. R. Kelly, I. Tellitu and J. P. Sestelo, *Angew. Chem.*, *Int. Ed. Engl.,* 1997, **36**, 1866.
18 (*a*) R.A. Bissell, E. Cordova, A. E. Kaifer and J. F. Stoddart, *Nature*, 1994, **369**, 133; (*b*) D. Philp and J. F. Stoddart, *Synlett.* 1991, 445; (*c*) A. C. Benniston, A. Harriman and V. M. Lynch, *J. Am. Chem. Soc.*, 1991, **117**, 5275.
19 E. Zahavy and M. A. Fox, *Chem. Eur. J.*, 1998, **4**, 1647.
20 (*a*) N. P. M. Huck and B. L. Feringa, *J. Chem. Soc.*, *Chem. Commun.*, 1995, 1095; (*b*) B. L. Feringa, W. F. Jager and B. de Lange, *J. Am. Chem. Soc.*, 1991, **113**, 5468.
21 (*a*) E. Katz and I. Willner, *Electroanalysis*, 1995, **7**, 417; (*b*) I. Moriguchi, K. Hanai, A. Hoshikuma, Y. Teraoka and S. Kagawa, *Chem. Lett.*, 1994, 691.
22 (*a*) E. Katz, M. Lion-Dagan and I. Willner, I. *J. Electroanal. Chem.*, 1996, **408**, 107; (*b*) E. Katz, A. L. De Lacey and V. M. Fernandez, *J. Electroanal. Chem.*, 1993, **358**, 261; (*c*) N. Nakashima and T. Tagushi, *Colloids Surf. A.*, 1995, **103**, 159.
23 (*a*) S. Shinkai, T. Minami, T. Kusano and O. Manabe, *J. Am. Chem. Soc.*, 1982, **104**, 1967; (*b*) M. Blank, L. M. Soo, N. H. Wassermann and B. F. Erlangler, *Science*, 1981, **214**, 70.
24 (*a*) M. P. Debreczeny, W. A. Svec and M. R. Wasielewski, *Science*, 1996, **274**, 584; (*b*) R. W. Wagner, J. S. Lindsey, J. Seth. V. Palaniappan and D. F. Bocian, *J. Am. Chem. Soc.*, 1996, **118**,

3996; (*c*) L. De Cola, V. Balzani, F. Barigelletti, L. Flamigni, P. Belser, A. Von Zelewsky, M. Frank and F. Vögtle, *Inorg. Chem.*, 1993, **32**, 5228.
25 A. Credi, V. Balzani, S. J. Langford and J. F. Stoddart, *J. Am. Chem. Soc.*, 1997, **119**, 2679.
26 (*a*) J. Daub, J. Salbeck, T. Knöchel, C. Fisher, H. Kunkely and K. M. Rapp, *Angew. Chem.*, *Int. Ed. Engl.*, 1989, **28**, 1494; (*b*) J. Daub, C. Fischer, J. Salbeck and K. Ulrich, *Adv. Mater.*, 1990, **2**, 366; (c) J. Achatz, C. Fischer, J. Salbeck and J. Daub, *J. Chem. Soc.*, *Chem. Commun.*, 1991, 504.
27 A. Ulman, *An Introduction to Ultrathin Organic Films from Langmuir–Blodgett to Self-Assembly*, Academic Press, San Diego, 1991.
28 (*a*) H. O. Finklea, in *Electroanalytical Chemistry*, vol. 19, ed. A. J. Bard and I. Rubinstein, Marcel Dekker, New York, 1996, pp. 109–335; (*b*) G. M. Whitesides and P. E. Laibinis, *Langmuir*, 1990, **6**, 87.
29 L. H. Dubois and R. G. Nuzzo, *Annu. Rev. Phys. Chem.*, 1992, **43**, 437.
30 (*a*) I. Willner, *Acc. Chem. Res.*, 1997, **30**, 347; (*b*) I. Willner and S. Rubin, *Angew. Chem.*, *Int. Ed. Engl.*, 1996, **35**, 367.
31 I. Willner and B. Willner, *Adv. Mater.* 1995, **7**, 587.
32 (*a*) I. Willner, M. Lion-Dagan, S. Marx-Tibbon and E. Katz, *J. Am. Chem. Soc.*, 1995, **117**, 6581; (*b*) M. Lion-Dagan, S. Marx-Tibbon, E. Katz and I. Willner, *Angew. Chem.*, *Int. Ed. Engl.*, 1995, **34**, 1604.
33 M. Lion-Dagan, E. Katz and I. Willner, *J. Chem. Soc.*, *Chem. Commun.*, 1994, 2741.
34 (*a*) I. Willner, R. Blonder and A. Dagan, *J. Am. Chem. Soc.*, 1994, **116**, 9365; (*b*) R. Blonder, S. Levi, G. Tao, I. Ben-Dov and I. Willner, *J. Am. Chem. Soc.*, 1997, **119**, 10467; (*c*) A. Bardea, A. Dagan, I. Ben-Dov, B. Amit and I. Willner, *Chem. Commun.*, 1998, 839; (*d*) A. Bardea, E. Katz, A. F. Bückmann and I. Willner, *J. Am. Chem. Soc.*, 1997, **119**, 9114.
35 I. Willner, G. Arad and E. Katz, *Bioelectrochem. Bioenerg.*, 1998, **44**, 209.
36 I. Willner and B. Willner, *Adv. Mater.*, 1997, **9**, 351.
37 (*a*) A. Doron, M. Portnoy, M. Lion-Dagan, E. Katz and I. Willner, *J. Am. Chem. Soc.*, 1996, **118**, 8937; (*b*) A. Doron, E. Katz, M. Portnoy and I. Willner, *Angew. Chem.*, *Int. Ed. Engl.*, 1996, **35**, 1535.
38 A. T. Hubbard, *Heterog. Chem. Rev.*, 1994, **1**, 3.
39 (*a*) E. Katz, N. Itzhak and I. Willner, *J. Electroanal. Chem.*, 1992, **336**, 357; (*b*) E. Katz, N. Itzhak and I. Willner, *Langmuir*, 1993, **9**, 1392.
40 (*a*) R. T. Lane and A. T. Hubbard, *J. Phys. Chem.*, 1973, **77**, 1411; (*b*) K. Takehara and Y. Ide, Y. *Bioelectrochem. Bioenerg.* 1992, **27**, 207.
41 F. Malem and D. Mandler, *Anal. Chem.*, 1993, **65**, 37.
42 A. Doron, E. Katz, G. Tao and I. Willner, *Langmuir*, 1997, **13**, 1783.
43 (*a*) M. Lahav, K. T. Ranjit, E. Katz and I. Willner, *Chem. Commun.*, 1997, 259; (*b*) M. Lahav, K. T. Ranjit, E. Katz and I. Willner, *Isr. J. Chem.*, 1997, **37**, 185.
44 (*a*) S. Marx-Tibbon, I. Ben-Dov and I. Willner, *J. Am. Chem. Soc.*, 1996, **118**, 4717; (*b*) K. T. Ranjit, S. Marx-Tibbon, I. Ben-Dov, B. Willner and I. Willner, *Isr. J. Chem.*, 1996, **36**, 407; (*c*) K. T. Ranjit, S. Marx-Tibbon, I. Ben-Dov and I. Willner, *Angew. Chem.*, *Int. Ed. Engl.,* 1997, **36**, 147.
45 I. Willner, Y. Eichen, M. Rabinovitz, R. Hoffman and S. Cohen, *J. Am. Chem. Soc.*, 1992, **114**, 637.
46 I. Willner, Y. Eichen, A. Doron and S. Marx, *Isr. J. Chem.*, 1992, **32**, 53.
47 E. Katz and I. Willner, *Langmuir*, 1997, **13**, 3364.
48 I. Willner, V. Pardo-Yissar, E. Katz, K. T. Ranjit, submitted for publication.

Feature Article 8/04135K